Relationship between Crystalline Structure and Mechanical Behavior in Isotropic and Oriented Polyamide 12

Nadya Dencheva[1], Zlatan Denchev*[1], M. Jovita Oliveira[1], Teresa G. Nunes[2], Sérgio S. Funari[3]

[1]IPC – Institute for Polymers and Composites, Department of Polymer Engineering, University of Minho, 4800-058 Guimarães, Portugal

[2]IST – Instituto Superior Técnico, Department of Materials Engineering and CQE, Av. Rovisco Pais 1, Lisboa, 1049-001, Portugal

[3]HASYLAB at DESY, Notkestraße 85, 22603 Hamburg, Germany

*Corresponding author: denchev@dep.uminho.pt

Revised version submitted to Journal of Applied Polymer Science on

November 2007

ABSTRACT

This study reports on the relationship between the crystalline structure and the mechanical behavior of differently processed and annealed polyamide 12 (PA12) samples. Two sets of samples were obtained: PA12 isotropic films prepared by hot pressing and oriented cables prepared by consecutive extrusion and cold-drawing. These samples were isothermally annealed in the 80 -160ºC range and then subjected to tensile tests at room temperature. A combination of solid state ^{13}C NMR and synchrotron wide- and small-angle X-ray scattering was used to obtain reliable structural data from these samples, before and after the tensile test. These structural data were related with the mechanical properties of the respective PA12 samples. Deformation models were suggested for the different PA12 samples explaining all the experimental results.

Key Words: polyamide 12, synchrotron WAXS and SAXS, mechanical properties, polymorphism, solid state NMR

INTRODUCTION

The properties of polyamide 12 (PA12) represent a valuable combination of the typical nylon and polyolefin properties, e.g. low moisture absorption and density accompanied by chemical resistance similar to that of polyamide 6 (PA6) with lower sensitivity to stress cracking[1,2]. PA12 shows excellent impact strengths and high E-modulus values. All this makes PA12 an important engineering plastic with multiplicity of applications in technical engineering, especially in automotive and electrical industries[3]. Therefore, studying the relationship between the PA12 structure and its mechanical properties has always been of both practical and academic interest.

It is generally accepted that polyamides possess layer-like structure formed by hydrogen-bonded sheets. The two basic crystalline modifications designated as α- and γ-forms were established for the first time in PA6[4-7]. It was demonstrated that, similarly to PA6, PA12 may also crystallize in α- and γ crystalline modifications, the latter being the more stable polymorph[8]. Depending on the crystallization conditions, four PA12 polymorphs were reported and designated as α, α′, γ and γ′. The main crystalline form obtained by melt crystallization of PA12 at atmospheric pressure was the γ-form, whereas the polymorph obtained by cryogenic quenching from the melt and subsequent crystallization at 60ºC was denoted as γ′-modification[9]. The α-polymorphs of PA12 are obtained under special conditions, e.g., crystallization from the melt at a pressure above 500 MPa[10], or precipitation from phenol-ethanol solution[11], or by drawing close to the melting point[12].

As regards the transitions between the four PA12 polymorphs, it was reported that thermal treatment under pressure gives rise to a γ′- to -α-form transition, whereas under the same conditions no change of the γ-crystalline form was established[10,13]. The γ′-structure can be transformed also into α- by annealing above 110ºC at atmospheric pressure[13]. The effect of drawing on the crystalline structure of PA12 was studied for the first time by means of wide

angle X-ray scattering (WAXS) by Northolt *et al*. [14]. The difference in the WAXS patterns before and after drawing was attributed to two different crystalline forms. Hiramatsu et al.[13] reported later that drawing above 50ºC and 70ºC could result in γ-γ′ or α-γ′ transitions, respectively. Ishikawa *et al.*[12] observed a partial γ- to α transition while drawing the PA12 sample at temperatures near the melting point.

Our own studies on the structure of PA12 displayed some differences in the polymorphic transitions occurring in the isotropic γ-form and in the oriented γ′form. Upon heating above 140ºC, the isotropic γ-polymorph partially changed into α-PA12 that only existed at high temperature and rapidly changed back into γ-form when cooled. No such γ- to α- transformation was observed with the oriented γ′PA12 phase even after annealing at temperatures close to melting. A γ'- to- γ transition was observed here only after isotropization by melting[15].

The present article is a part of a broader study on the structure-properties relationship in in-situ composite materials based on polymer blends containing PA12. It reports on the mutual relationship between the structure in the crystalline and amorphous domains and the mechanical behavior in well-characterized, differently annealed, oriented or isotropic PA12 samples containing various amounts of α- and γ-polymorphs. To the best of our knowledge, no such studies have been published so far with PA12. The influence of the starting structure upon the mechanical properties of PA12 samples is studied. Then, the influence of strain after sample failure considering the changes in the crystalline and amorphous phases is elucidated. Synchrotron WAXS and small-angle X-ray scattering (SAXS) were used, complemented by solid state ^{13}C NMR spectroscopy allowed for verifying the type and content of the respective polymorphs.

.

EXPERIMENTAL

Materials Used and Sample Preparation

High viscosity grade PA12 obtained by ring-opening polymerization and commercially available under the trade name *Grilamid L25* (EMS Grivory, Switzerland) with a density of 1.01 g/cm^3; $\overline{M}_w$ = 60.000; $\overline{M}_n$ = 31.000; melting point T_m = 178ºC (DSC) was used as a starting material.

Two types of PA12 samples were prepared and studied. The first one, designated as "isotropic film", was obtained by compression molding of as-supplied granules preliminarily dried for 5 h at 90ºC. The starting material was pressed at 250ºC, and a pressure of 6 tons was applied for 5 min, which was followed by isothermal crystallization for 1 h at three different temperatures: 120, 140, or 160ºC. An additional sample was prepared with 3 h of isothermal crystallization at 120ºC. After completing the annealing, 200–250 μm thick films were prepared by cooling to room temperature at a rate of about 20ºC/min. Five standard specimens for tensile stress measurements with 25 mm length and 4 mm width were cut out from each film.

The second set of samples, designated as "oriented cables" (OC), was prepared in an extruder line including a Lestritz LSM 30.34 intermeshing co-rotating twin-screw extruder, two water baths, two haul-off units and a winder positioned downstream. The extrusion was performed at a set temperature of 230ºC. The extrudate was cooled in the first water bath down to 12ºC while drawing it at a draw ratio (DR) of ca. 3.0. The final drawing was performed in the second haul-off unit after heating the stretched cable up to 90-96ºC in the second water bath. More details about the extruder line can be found elsewhere[16]. The PA12 OCs were annealed with free ends at 80, 100, 120, and 160ºC in an oven. After 1 h of annealing at the respective temperature, the sample was cooled at about 10ºC/min until it

returned to room temperature. Major sample contraction was observed in each annealing temperature with all PA12 oriented cables.

Solid state NMR

Solid state NMR measurements were performed in a Bruker MSL300P spectrometer operating at 75.47 MHz for the observation of ^{13}C resonances, using Magic-Angle Spinning (MAS), high-power ^{1}H Dipolar Decoupling (DD), and ^{1}H-^{13}C Cross-Polarization (CP) combined techniques. The ^{1}H-^{13}C CP contact time was 1 ms giving a good discrimination of the protonated signals. The maximum inter-radio frequency pulse sequence delay was 3.0 s at a spinning rate of 3.4 kHz. The B_1 Radio Frequency field intensity was 55 kHz and the number of scans varied between 1000 and 2000. Glycine signals were employed as external references for determination of the chemical shifts with an accuracy of 0.2 ppm. The temperature of the probe head was set to 20 ± 1ºC. The experimental spectra were fitted by individual Gaussian peaks using commercial peak fitting software.

WAXS and SAXS Measurements

Synchrotron radiation with a wavelength of 0.15 nm generated at the Soft Condensed Matter Beamline (A2) of HASYLAB, Hamburg, Germany was employed. The first setup used permitted two-dimensional (2D) SAXS and 1D WAXS measurements. The sample-to-detector distance for SAXS was set to 2850 mm, the diffraction patterns being registered by means of a MARCCD 2D detector with exposure times between 30 and 90 sec. The 1D WAXS profiles were registered by a linear scintillation detector positioned at 240 mm in respect to the sample holder. In the second setup for 2D WAXS, the linear detector was removed and the MARCCD detector was positioned at 90 mm from the sample. More details on the setups employed may be found elsewhere[15].

SAXS and WAXS data handling

Data handling procedures were performed as previously described[15-18]. All SAXS and WAXS patterns were corrected for background scattering, constant sample thickness and beam intensity. The scattering angle axis for WAXS was calibrated using the angular position of the reflections of a standard crystalline poly(ethylene terephthalate) sample. Calibration of the SAXS scattering angle axis was made by a rattail standard sample.

All WAXS curves were fitted with Gaussian peaks. In the case of isotropic PA12 the total degree of crystallinity (or, crystallinity index, CI) was calculated as a relation of the areas of all crystalline peaks and the total area underneath the WAXS curve:

$$CI = \frac{\sum A_c}{\sum (A_c + A_a)} \tag{1}$$

There, A_c is the integrated area underneath the respective crystalline peaks and A_a is the integrated area of the amorphous halo.

In PA12 oriented cables, the intensity of the meridional point-like reflections cannot be determined from the 1D WAXS curves. In this case, ΣA_c in Eq. 1 measures the scattering intensity along the equator only, *i.e*. Eq. 1 would represent the "equatorial crystallinity index" (ECI).

The 1D WAXS patterns were used also to determine the interplanar spacings d_{h00} and d_{00l} using the Bragg´s law:

$$2d_{hkl} \sin\theta_{hkl} = \lambda \tag{2}$$

Here, λ = 1.5 Å is the X-ray wavelength and θ is the half of the 2θ position of the center of the respective crystalline peak.

Tensile Tests

Uniaxial tensile tests were performed in an Instron model 4505 machine. The tests were carried out at 23 ± 2ºC with a load cell of 1 kN at constant crosshead speed of 50 mm/min. The nominal stress was determined as a ratio of the tensile force and the initial cross section of the sample. The nominal strain was determined as a ratio of the sample gauge length at any time during drawing and that prior to drawing.

RESULTS

Mechanical Data

Figure 1 shows the stress–strain curves of differently annealed isotropic PA12 films (a) and oriented cables (b). All data extracted from these curves are presented in Table 1.

As seen from Fig. 1 (a), all isotropic PA12 samples display clear yield points at low strains (between 7 and 9%) and cold flow regions – a behavior typical of necking. The samples annealed at 120/1h and 140ºC failed at strains at break, ε_{br} of ca. 200%, whereas the other two films broke at ε_{br} values of 50-60%. From Table 1 it can be seen that the isotropic PA12 samples displayed a slight augmentation of the Young modulus E - from 830-890 MPa to 1030 MPa. This effect was achieved by increasing either the annealing temperature T_a in the 120 - 160ºC range, or the duration of the treatment – from 1 to 3 h at 120ºC. The yield stress (σ_y) values of all isotropic samples were between 32 and 36 MPa, the highest value corresponding to the highest annealing temperature of 160ºC. It can be concluded that annealing results in a harder PA12 film.

Fig. 1 (b) shows that all oriented PA12 cables are characterized by two yield points. As seen from the data in Table 1, the first yields appear at low strains (3-5%) with σ_y values between 45 and 59 MPa. At strains of 16-21% one can recognize in all OCs a second yield

point with σ_y values in the 207-254 MPa. Statistically significant increase of the *E* modulus values here was reached only at annealing temperatures of 140º and 160ºC; at lower temperatures the mechanical behavior of the annealed OCs is similar to that of the OC without annealing.

(Figure 1)

(Table 1)

Solid State ^{13}C NMR Data

In our previous study[15], the solid state NMR spectra of PA12 granules and PA12 cable obtained by melting the same granules in a melt flow index apparatus followed by stretching at ca.100ºC, did not reveal any resonance lines above 40 ppm and also no peaks around 38.9–39.0 ppm. On this basis, the presence of α-polymorph in both samples was ruled out. For the mechanical experiments in this work isotropic films were prepared by hot pressing and OCs – using the extruder line with two stretching devices. The MAS/CP-DD ^{13}C NMR spectra of a PA12 isotropic film annealed for 1 h at 160ºC and of the new OC with the same thermal prehistory obtained before and after the tensile test of the samples were visibly different from those of the previous study. Having in mind also the prolonged annealing of the samples at elevated temperatures, we decided to analyze the new NMR data by peak-fitting supposing the presence of both α and γ-PA12 polymorphs. This hypothesis was based on the previous works reporting on γ- to α-form transition upon cold drawing[12] or pressing[13]. The crystallinity data obtained by fitting the NMR curves were then correlated with the X-ray scattering results.

Fitting of the NMR spectra is possible having in mind the four types of aliphatic carbons found in the repeat unit of both α- and γ-PA12 (Table 2).

(Table 2)

In each polymorph, its eight CH_2 methylenes (type **c** carbons) co-exist in all-trans and in gauche (skewed) conformations, the resonances of these structures being in the 30.3-34.3 ppm range. The methylene type **b** carbon, being the most electron-shielded, appears in stronger fields of ca. 27 ppm. As expected, the carbon located next to the C=O and that next to the NH group (type **a** and **d**, respectively) produce resonance lines in weaker fields (up to 43 ppm).

Figures 2 and 3 represent the fittings of the extended methylene carbon regions of an isotropic PA12 sample annealed for 1h at 160ºC and an OC with the same thermal history before (a) and after tensile test (b). The respective chemical shifts obtained after the peak fitting for all types of carbons are presented in Table 2. They are very close to those found previously[19].

(Figure 2)

(Figure 3)

Fitting the NMR spectra allows the calculation of the α/γ polymorph ratio, which was done in the following way. The areas of all-cis and all-trans methylene carbon γ-PA12 peaks were summed and divided by 8 obtaining in such a way the integral intensity corresponding to one γ-carbon. This value was then used to divide the integral intensity of the **d**-type carbon of the α-PA12. One has to mention that it is possible to calculate the α/γ ratio relating the intensity of any NMR signal of a carbon belonging to α-PA12 with that of any carbon of the γ-phase. In all cases very similar values were obtained. We preferred to use the signal of the α-PA12 **d**–carbon because of two reasons. This signal appears above 40 ppm where there are no γ-form signals whatsoever so the presence of it undoubtedly proves the α-form. Below 40 ppm superposition is possible between α- and γ-form signals. The second reason was the better agreement with the WAXS data.

1D WAXS Measurements

As seen from the comparison between the literature and our chemical shift data presented in the Table 2, in isotropic PA12 films and PA12 OCs a clear distinction is possible between the α- and γ PA12 phases. However, no distinction was possible between the γ- and γ'-PA12. That is why in this work when referring to oriented PA12 samples, we will have in mind the γ'-oriented PA12 phase; the isotropic PA12 films will be considered then as containing γ-type isotropic phase only.

Figure 4 shows the fitted 1D WAXS patterns of the same isotropic and oriented PA12 samples studied by solid state NMR. All fits were made with 5 Gaussians – two for the monoclinic α-polymorph, two for the pseudo-hexagonal γ-type isotropic polymorph and one broad peak for the amorphous halo. Comparing the shape of the patterns allows the conclusion that the isotropic and oriented PA12 have different crystalline structures. The centers of the amorphous halo in the isotropic sample (Fig. 4 (a)) do not coincide with the main crystalline peaks as in PA12 with orientation (Fig. 4 (b-d)).

From the shapes of the 1D WAXS patterns of the oriented samples it is not straightforward whether or not they should be fitted with crystalline peaks for the α-phase. This becomes evident only on the basis of the NMR results shown in Table 2. It is worth noting that the α/γ ratios obtained from the WAXS patterns of the isotropic and oriented PA12 samples annealed at 160ºC before and after tensile test almost coincide with those obtained with the same samples by fitting their NMR patterns. Therefore, the procedure of fitting of these particular WAXS curves was extended to all 1D WAXS patterns. The structural data obtained in such a way are presented in Table 3.

(Figure 4)

(Table 3)

As seen from Table 3, annealing of isotropic PA12 samples results in a small increase of CI, better expressed for the γ-crystals. Stretching during the tensile test resulted, as a rule, in strain-induced crystallization of amorphous material predominantly in α-form. With the PA12 OCs, when increasing the annealing temperature in the 80-140ºC range, a significant increase in ECI of ca. 11% was produced. The small drop in ECI at 160ºC, which is 15 degrees below T_m of PA12 should be attributed to some melting/recrystallization processes. The tensile test with the differently annealed OCs resulted in a general γ-to α-transition maintaining almost the same ECI values as before tensile test.

2D WAXS measurements

The crystallinity indices in Table 3 and the most of the d-spacings data in Table 4 were obtained on the basis of the 1D WAXS patterns. The latter, however, account only for the equatorial WAXS reflections. It is known from previous studies that the oriented γ-PA12 displays also meridional point-like reflections. Therefore, 2D WAXS patterns were obtained from which the $d_{\gamma 020}$ were determined for some PA12 samples, before and after tensile test. The most representative 2D WAXS patterns are shown in Fig. 5.

(Table 4)

(Figure 5)

The first pattern in Fig. 5 is isotropic. The equatorial cut of its external ring produces the pattern in Fig. 4 (a). The internal ring is related with $d_{\gamma 020}$ and is also quite isotropic. The pattern in Figure 5 (b) proves the strong orientation in the PA12 OCs, the draw direction (DD) being vertical. Drawing the PA12 films to sample failure during the tensile test transforms the isotropic pattern in Fig. 5 (a) into the well-oriented pattern in Fig. 5 (c), which indicates that the external force is transferred to the crystallites. The 2D WAXS patterns of PA12 OCs upon

drawing do not change their symmetry, only the scattering intensity decreases most probably due to smaller sample cross-section.

As seen from Table 4, increasing the annealing temperature of PA12 films in the 120 - 160ºC region leads to a decrease of $d_{\alpha 200}$, $d\gamma_{001}$ and of $d_{\gamma 020}$ values while the rest of the d-spacings remain constant. Drawing the films to sample failure results, generally, in a well-expressed growth of all d-spacing obtained from the equatorial reflections, whereas the $d_{\gamma 020}$ values drop. With the oriented PA12 samples, a clear trend toward diminution of $d_{\alpha 200}$ and $d_{\gamma 020}$ as a function of the annealing temperature was registered, the rest of the d-spacings remaining constant. The application of external force changes only the $d_{\gamma 020}$ values best revealed in the OC without annealing.

2D SAXS measurements

The evolution of the 2D SAXS patterns in isotropic and oriented PA12 samples as a function of the annealing temperature before and after tensile test is given in Figure 6. All PA12 initial films display isotropic patterns similar to that in Fig. 6 (a). After the tensile test, the films annealed for 1 h at 120 and 140ºC produce clear four-point scattering diagrams with fiber structure (Figure 6.b), whereas the PA12 films with 3 h at 120ºC and 1 h at 160ºC show only a vertical central streak and no evidence of coherent scattering at larger s-values (Fig. 6 c).

The OCs have a completely different nanostructure (Fig. 6 (d - f)). The as-drawn cable and that annealed at 80ºC show only a central streak (Fig. 6. d), both before and after the tensile test. Annealing in the 100-160ºC interval results in the appearance of coherent scattering typical of microfibrilar structure (Fig 6 e), whose form does not change after the mechanical test (f).

(Figure 6)

More structural information can be extracted from the above 2D patterns after their processing: scanning the intensities in radial direction provides quantitative information about the Bragg's long spacing (L_B) values and sample's scattering power, while the angular scan shows the intensity distribution in a given azimuthal angular range. Fig. 7 and Fig. 8 display these data for PA12 films and OC respectively as a function of the annealing temperature, before and after tensile test. Table 5 summarizes the L_B values of all samples studied.

(Table 5)

(Figure 7)

(Figure 8)

Analyzing Figs. 7 and 8, (the curves in (a) and (b)) shows that increasing the annealing temperature above 100ºC results in a gradual increase of all L_B values (Table 5) and of the scattering power, especially at 160ºC. Stretching to mechanical failure in PA12 films leads, in general, to significantly lower scattering intensities and lower L_B values (1h/120 and 1h/140ºC) or to complete disappearance of coherent scattering (3h/120, 1h/160ºC). As seen from Fig. 7 (c), with these two samples, the external load applied resulted in clear bimodal distribution of the scattered intensity with peaks at azimuthal angles φ = 45 and 60º, respectively, φ being the angle between DD and the normal to the lamellae surface (Fig. 6).

Similar trends were revealed with the OCs. (Fig. 8 a, b), with the notable exception of the sample with 1h at 140ºC that after the tensile test displayed higher scattering strength as compared to that of the initial OC. The azimuthal scans of all OC patterns before and after the tensile test revealed curves very similar to those in Fig. 8 (c) indicating a four-point scattering diagram with φ = 30º.

DISCUSSION

PA12 Isotropic Films

Analyzing the stress–strain curves in Fig. 1(a) and the numeric data in Tab. 1, it becomes evident that the annealed isotropic PA12 samples studied can be divided into two groups. Within each group the mechanical properties can be considered very similar. Thus, annealing for 1h at 120ºC and 140ºC results in ε_{br} values in the 190 - 200% range, σ_y being of ca. 32 MPa and the *E* values below 900 MPa. With the other two films annealed for 3h at 120ºC and 1h at 160ºC respectively, the ultimate strain drops to 50-60%. At the same time, *E* goes above 1.0 GPa and σ_y also grows to ca. 35 MPa.

Relating the above mechanical behavior to the degree of crystallinity and the polymorph type (Table 3) before tensile test is not straightforward. On the one hand, increasing T_a from 120 to 160ºC results in a 6% growth of CI_{total}, the largest difference being between 140 and 160ºC. On the other hand, the α/γ content has its maximum at 140ºC and goes back to the initial values of ca. 0.20 at 160ºC. None of these changes can be linked directly to the mechanical performance of the respective samples. At the same time, however, Table 4 shows that increasing T_a and its time duration leads to slight but observable decrease of $d_{\alpha 200}$, $d_{\gamma 001}$ and $d_{\gamma 020}$ values. In the case of $d_{\alpha 200}$ and $d_{\gamma 001}$ this would mean a drop of the H - bond lengths within the α-PA12 and γ-PA12 sheets respectively. In the case of $d_{\gamma 020}$, one deals with a well-expressed shrinkage of the γ-type unit cell along the chain axis. Both effects are related to a denser packing of the macromolecules in the crystalline domains, which is a probable explanation of the increase of σ_y as the T_a grows.

All initially isotropic PA12 films after the tensile test showed 2D WAXS patterns with fiber symmetry similar to that in Fig. 5 (c) indicating strong orientation of the crystallites

along DD. Most all d-spacings increase after tensile test (Table 4) suggesting a stress-induced unit cell expansion. Only the $d_{\gamma 020}$ displays some decrease. The same effect was observed in oriented PA6, too[18]. At this point this experimental fact is not well understood.

The 2D and 1D SAXS data provide additional help in trying to understand the structure-properties relationship in isotropic PA12 films before tensile test. Figs. 6 (a) and 7 (c) show that before the tensile test the PA12 films can be considered isotropic with an almost uniform distribution of the scattered intensity along the circular 2D SAXS pattern. As a result of annealing, the scattering strength increases – gradually between 120 and 140ºC and with an abrupt jump between 140 and 160ºC (Fig. 7 (a)). Exactly in the same way the respective L_B values grow (Table 5). Having in mind the CI_{total} values at the latter two temperatures (33.5 and 37.3%), the significant increase in L_B with 30 Å could hardly be attributed to lamellar thickening only, i.e., to changes exclusively in the crystalline domains. Considering also the mechanical data, a more logical explanation would be the supposition that annealing for 1h at $T_a >$ 140ºC or for 3h at 120ºC results in the formation of certain amounts of rigid amorphous phase that cannot be detected by WAXS, whose density, however, is very similar to that of the crystalline domains and is registered by SAXS.

We believe that the structural data after tensile test support the supposition of amorphous phase hardening above certain T_a. As already mentioned, the samples annealed for 1h at 120 and 140ºC have similar ε_{br} of ca. 190 and 200%, as compared to the 50-60% of the samples with 3h at 120 and 1h at 160ºC. This observation can be explained by the well-known concept that deformation of semicrystalline polymers takes place by unfolding of the flexible macromolecules found in the disordered domains between the stiff ordered crystalline regions. Apparently, more flexible amorphous domains would correspond to higher ε_{br} values and vice versa.

A logical consequence of the above concept is that a part of the external force applied during the tensile test would be transferred to the crystalline domains thus enabling stress-induced structural changes. Comparing the α/γ content before and after tensile test (Table 3) suggests that the strongest γ- to α- transition as a result of drawing is registered after 1h at 120ºC and the lowest – after 1h at 160ºC. This leads to the unexpected conclusion that more flexible disordered domains would transfer to the adjacent crystalline domains a bigger part of the external force. The evolution of σ_{br} as a function of T_a (Table 1) helps explain this apparent paradox. Due to strain hardening, the films annealed for 1h at 120 and 140ºC have reached higher σ_{br} values that have intensified the stress-induced γ- to α-polymorph transition.

More evidence of the appearance of rigid amorphous phase as a result of annealing is found in the SAXS data in Figs 6 and 7. After the tensile test the PA12 films annealed for 1h at 120 and 1h at 140ºC reveal four-point patterns similar to that in Fig. 6 (b). The structure that gives rise to such patterns is still being debated. According to some authors, the lamellar surface can tilt because of the progressive shear between the crystalline stems within the lamellae[20-22]. In this model, a two- or a four-point pattern is obtained depending on whether this surface is perpendicular or tilted away from the chain axis (in this case coinciding with DD), respectively. In a second group of models[23,24], a four-point pattern is obtained when the lamellae are arranged in a lattice that resembles a checkerboard, and a two-point pattern is obtained when the lamellae are arranged in columns and the positions of the lamellae in the neighboring columns are not correlated. A recent extensive SAXS study on the deformation behavior of some thermoplastic polymers combines the above two models. Thus, samples subjected to high deformations (250 - 500%) and thereafter unloaded consist of parallel crystalline lamellae tilted with respect to DD. Under stress, however, there occurs a disruption of the tilted lamellae into smaller pieces. These fragments form a macrolattice with hexagonal order. When the elongation is increased beyond 250%, the lattice is transformed

into an ensemble of microfibrils with little correlation in lateral direction giving rise to a two-point (lobe type) pattern[25]. Another combined model explaining the four-point pattern in strained homopolymers was proposed very recently by Murthy and Grubb[26] introducing the concept of a 3D lattice of tilted lamellae. A transition from four-point to two-point SAXS diagram was also observed by Hernandez et al by stretching of a poly(ether ester) block copolymer with and without carbon nanotubes reinforcement[27].

To explain the four-point patterns in the films annealed at 120ºC/1h and 140ºC/1h after the tensile test, we supposed the presence of flexible amorphous phase. The simplified scheme in Fig. 9 visualizes the application of the tilted lamellae deformation model with these samples. Underneath the cartoons of the respective lamellar structures, the scattering patterns produced by them are given.

(Figure 9)

Straining the isotropic PA12 films with flexible amorphous phase during the mechanical test causes the arrangement of the random lamellae (1) into lamellar stacks oriented perpendicularly to DD (2). The latter is present while the sample is still under stress in the testing machine. After sample failure, rupture of the tie molecules between the crystalline domains occurs. The release of the external force allows for the said lamellar tilt to take place. From the azimuthal scans in Fig. 7 (c) it was found out that the lamellar tilts are at ca. 45 (1h/120º) and 60º (1h/140ºC). This is accompanied by a measurable decrease of L_B which is expectable in the case of relaxation. Fig. 7 (b) shows also that stretching of the latter PA12 films results in a loss of scattering power.

After stretching of the harder PA12 films (3h/120ºC and 1h/160ºC) a complete loss of coherent SAXS scattering is observed (Figs. 6 c, 7 b). The reason for this effect cannot be the disappearance of the denser domains since the CI_{total} of the stretched samples increases as compared to that in the respective samples before the tensile test. Most probably, as a result of

stretching along the chain axis, the L_B values become too large to be registered by a sample-to-detector distance of 2.8 meters. Evidently no relaxation with L_B decrease could occur after stress release. This fact supports the hypothesis that harder amorphous phase is produced at higher T_a or longer annealing times in PA12 films.

Oriented PA12 cables

The stress–strain curves of all PA12 cables [Fig. 1 (b), Table 1] were characterized by double yield. The two σ_y values change with T_a reaching the highest values after annealing at 140ºC but it is difficult to trace any proportionality between these two parameters. All PA12 cables display similar ductility. As expected, the biggest ε_{br} was shown by the OC without annealing, and the smallest – by the OC annealed at 160ºC. The *E* values were also affected by the annealing: in principle, the higher the T_a was, the bigger *E* values were obtained.

Comparing the mechanical data of the OCs in Table 1 to the structural data extracted from the crystalline phase in Table 3 shows that the highest ultimate stress values of 266 MPa was obtained with the OC annealed at 140ºC, which has the highest ECI of ca. 53% containing at the same time the highest percentage of γ-polymorph – close to 40%. Any decrease of ECI led to diminution of the ultimate stress values. Annealing temperature of 160ºC seems to be higher than the optimum causing some loss of crystallinity directly reflecting in lower stress values (Tables 1. and 3) Annealing the OCs in the 80-160ºC leads to a general decrease of the $d_{\alpha 200}$ and $d_{\gamma 020}$ values indicating a denser packing of the macromolecules. As expected, all 2D WAXS patterns display a strong orientation along the DD (Fig. 5). This observation was confirmed by the 2D SAXS patterns in Fig. 6. Some coherent scattering of lamellar structures was revealed only after annealing of the OCs at T_a>100ºC. As in the previous section, increasing the annealing temperature increases the

scattering power of the OC before mechanical test (Fig. 8 a). The jump in the scattered intensities between 1h at 140 and 160ºC was again attributed to the formation of rigid amorphous phase not detectable by WAXS.

All curves obtained by azimuthal cuts of the 2D SAXS patterns of OCs annealed above 100ºC are similar to that in Fig. 8 (c), which exemplifies the sample annealed at 160ºC. These curves are different from those of the soft PA12 films after the tensile test (Fig. 7 c). The latter can be fitted with two Gaussians without any peak centered at 0º thus indicating a "pure" four-point pattern attributable to the presence of tilted lamellae (Fig. 9). The curves of the OCs in Fig. 8 (c) need to be fitted with three Gaussians, the middle one being at 0º in respect to the chain axis direction. This finding supports the coexistence of two- and four-point patterns in the oriented PA12 samples. As mentioned above, such patterns are typical of oriented semicrystalline fibers under stress whose scattering elements are arranged in a macrolattice. Figure 10 gives a schematic representation of the various structures and the respective SAXS patterns in PA12 OCs.

(Figure 10)

The initial OC without annealing as obtained in the extruder line is characterized by a nanostructure composed of laterally uncorrelated fibers with very large long spacings impossible to register with the maximum sample-to-detector distance in the beamline used. The scattering pattern is supposed to be of two-point type with its lobes being hidden behind the beamstop (cartoon 6 in Fig 10). Annealing the OCs with free ends at a $T_a \geq 80$ºC results in relaxation whose macroscopic effect is the strong cable contraction observed with all OCs upon heating with a drop in L_B being sufficient to reveal coherent SAXS scattering. Moreover, the significant increase in ECI registered in samples annealed at $T_a \geq$ 100ºC (Table 3) may be related to the formation of some new crystalline domains of α-type appearing in the amorphous regions between the lamellae and leading to macrolattice

formation similar to Fig. 10, cartoon 5. As a result, the L_B values drop significantly making possible their registration. The SAXS patterns display coexistence of two- and four-point patterns. As seen from Table 5, increasing the T_a to 140 and especially to 160ºC starts a trend toward L_B growth. Based on the ECI data (Table 3), this effect can be explained with lamellar thickening (up to 140ºC) or with incipient fusion of some elements of the macrolatttice (at 160ºC), apparently from the α-PA12 polymorph.

With the PA12 OCs we did not observe pure two-point patterns corresponding to structure 4 in Fig. 10. The reason is that such a structure is expected at relatively low deformations. The preparation of OCs includes cold drawing to high DR causing irreversible disruption of the crystalline lamellae to form fibrillar structure. However, undisrupted oriented lamellar stacks giving two-point patterns have been undoubtedly registered at low deformation rates (ca 50%) with a number of thermoplastic neat polymers and segmented copolymers[25].

All OCs display ε_{br} values between 20 and 30%. Straining during the mechanical test leads to a well-pronounced γ- to α-form transition (Table 3). As seen from Fig. 8 (b), stretching results in a decrease of the scattering power with T_a of 100 and 120ºC as compared to the respective values before tensile test (Fig. 8 a). With the samples annealed for 1h at 140ºC and 160ºC there is an increase of the scattered intensity, much stronger in the former case. These results can be explained with the formation of additional amounts of rigid amorphous phase. As seen from Table 5, there are no changes in L_B after the mechanical test, i.e. relaxation does not occur upon sample failure in any of the OCs. This finding could be related to an amorphous phase being hard enough to prevent any significant shrinkage of the microfibrils even at the lowest annealing temperature. This is in good agreement with the fact that the d-spacings of all OCs before and after tensile test do not change significantly (Table

4). The only exception is the $d_{\gamma 020}$ value dropping strongly upon sample failure, the reason for which is not well understood at this point.

CONCLUSIONS

The PA12 isotropic films obtained by the compression molding and the PA12 oriented cables obtained by consecutive extrusion and cold drawing contained predominantly the γ-crystalline form with some amounts of PA12 α-modification, the fraction of the latter being larger in the oriented samples. The combination of ^{13}C solid state NMR with WAXS and SAXS from synchrotron was very useful for obtaining of reliable structural information about the polymorph transitions in PA12. Thus, the annealing applied caused an additional γ-to-α form transition expressed in an increase of the α/γ content. Both isotropic and oriented PA12 samples showed a growth in the E and σ_y values, as well as a decrease in ε_{br} values as the annealing temperatures increased. This behavior was explained, on a crystallographic level, by a denser packing of the macromolecules in the crystalline domains. All structural data obtained allowed the supposition of formation of rigid amorphous phase in the annealed samples. The external stress applied during the tensile test led to additional stress-induced γ-to α-form transitions in all PA12 samples accompanied by changes of the respective nanostructures.

ACKNOWLEDGEMENTS

This work was supported by the IHP-Contract HPRI-CT-2001-00140 of the European Commission and the HASYLAB Project II-04-047 EC. A partial financial support was provided by FCT project POCI/CTM/57358/2004. N.D. thanks for the financial support of her PhD research by grant No SFRH/BD/13435/2003 awarded by *Fundação para a Ciência e Tecnologia*, Portugal

.

REFERENCES

1. Ulf, H; Rohde-Liebenau, W. Nylon 12 in: *Polymer Data Handbook*, ed by Mark JE, Oxford University Press, New York, 1999, pp. 225-229.
2. Aharoni, S. M. n-Nylons, Their Synthesis, Structure and Properties, John Wiley & Sons: New York, 1997, p. 316-317.
3. Kohan MI, *Nylon Plastics Handbook,* Hanser Publishers, Munich (Hanser/Gardner Publications, Cincinnati), 1995.
4. Holmes, D.R.; Bunn, C. W.; Smith, D. J. J Polym Sci 1955, 17, 159-177.
5. Arimoto, H.; Ishibashi, M.; Hirai, M.; Chatani, Y. J Polym Sci Part A: Polym Chem 1965, 3, 317-326.
6. Fornes, T. D.; Paul, D. R. Polymer 2003, 44, 3945–3961.
7. Samon, J. M.; Schultz, J. M.; Hsiao, B. S. Polymer 2000, 41, 2169–2182.
8. Aleman, C.; Casanovas, C. Colloid Polym Sci 2004, 282, 535-543.
9. Li, L.; Koch, M.; de Jeu, W.H. Macromolecules 2003, 36, 1626-1632.
10. Hiramatsu, N.; Hashida, S.; Hirakawa, S. Jpn J Appl Phys 1982, 21,651-654.
11. Ishikawa, T.; Nagai, S.; Kasai, N. J Polym Sci Part B: Polym. Phys Ed.1980, 18, 291-299.
12. Ishikawa, T.; Nagai, S.; Kasai, N. Die Makromol Chem 1981, 182, 977 – 988
13. Hiramatsu, N.; Haraguchi, K.; Hirakawa, S. J Appl Phys 1983, 22, 335-339.
14. Northolt, M. G.; Tabor, B. J.; van Aartsen, J. J. J Polym Sci Part A-2: Polym Phys 1972, 10, 191-192.

15. Dencheva, N.; Nunes, T.; Oliveira, M. J.; Denchev, Z. J Polym Sci Part B: Polym Phys 2005, 43, 3720-3733.

16. Denchev, Z.; Oliveira, M. J.; Carneiro, O. S. J Macromol Sci Part B: Physics 2004, B43, 143-162.

17. Dencheva, N.; Denchev, Z.; Oliveira, M. J.; Funari, S. S. J Appl Polym Sci 2007, 103, 2242-2252

18. Dencheva, N.; Nunes, T.; Oliveira, M.J.; Denchev, Z. Polymer 2005, 46, 887

19. Mathias, L. J.; Johnson, C.G. Macromolecules 1991, 24, 6114.

20. Pope, D.P.; Keller, A. J Polym Sci Polym Phys Ed 1975, 13, 533.

21. Matyi, R.J.; Crist, B.Jr. J Polym Sci Polym Phys Ed 1978,16, 1329.

22. Murthy, N.S. ; Grubb, D.T. J Polym. Sci Phys Ed 2003, 41, 1538-1553..

23. Statton, W.O. J Polym Sci 1959, 16,143.

24. Wilke, W.; Bratrich, M. J Appl Cryst 1991, 24, 645.

25. Stribeck, N.; Fakirov, S.; Apostolov, AA.; Denchev, Z.; Gehrke, R. Macromol Chem Phys 2003, 204:1000.

26. Murthy, N.S.; Grubb, D.T. J Polym. Sci Phys Ed 2006, 44, 1277-1286.

27. Hernández, J.J.; García-Gutiérrez, M.C.; Nogales, A.; Rueda, D.R.; Sanz, A.; Sics, I.; Hsiao, B.S.; Roslaniec, Z.; Broza, G.; Ezquerra, T.A.. Polymer 2007, 48, 3286-3293.

IMAGE TEXTS

Figure Captions

Figure 1 Stress–strain curves of various PA12 samples: (a) isotropic films annealed for 1 h at 120, 140, or 160ºC, and for 3 h at 120ºC; (b) oriented PA12 cables without annealing (w.a.) and annealed at 80, 100, 120, and 140ºC for 1 h. The curves represented were selected to best fit the averaged data in Table 1.

Figure 2 Aliphatic atom region of the MAS/CP-DD ^{13}C spectra at 20ºC of isotropic PA12 film annealed for 1h at 160ºC: (a) before and (b) after TT. The resolved resonance lines of the α-PA12 are shaded. The chemical shifts of all resonance lines are given in Table 2. (TT = tensile test)

Figure 3 Aliphatic atom region of the MAS/CP-DD ^{13}C spectra at 20ºC of PA12 OC obtained by extrusion/cold drawing and annealed for 1h at 160ºC: (a) before and (b) after TT. The resolved resonance lines of the α-PA12 are shaded. The chemical shifts of all lines are given in Table 2.

Figure 4 1D WAXS patterns of PA12 samples annealed for 1 h at 160ºC and their fitting with Gaussian peaks: PA12 film before (a) (and after (b) TT; PA12 OC before (c) (and after (d) TT. The peaks of the α-PA12 are shaded. The amorphous halo was modeled by one Gaussian.

Figure 5 2D WAXS patterns of: (a) PA12 film annealed for 1h at 160ºC; (b) oriented PA12 cable, without annealing; (c) sample (a) after the tensile test. All patterns are obtained at 30ºC. The draw direction in (b) and (c) is vertical and **b** axis is the chain axis.

Figure 6 2D SAXS patterns of: selected isotropic films (a – c) and OCs (d - f) with various annealing before and after TT: (a) isotropic film, 1h at 140ºC; (b) sample (a) after TT; (c) film 1 h at 160ºC, after TT; (d) OC without annealing; (e) OC 1h at 160ºC; (f)

sample (e) after TT. All patterns are obtained at 30ºC. The draw direction in oriented patterns is vertical.

Figure 7 Slicing of 2D SAXS patterns of initially isotropic PA12 films: (a) Raw 1D SAXS profiles as a function of the annealing temperature and duration, before TT; (b) same as (a), after TT; (c) azimuthal scans in the -90 – +90º range for samples with: 1 - 1h at 120ºC and 2 - 1 h at 140ºC. Open symbols – before TT, solid symbols – after TT.

Figure 8 Slicing of 2D SAXS patterns of PA12 OCs: (a) Raw 1D SAXS profiles as a function of the annealing temperature and duration, before TT; (b) same as (a), after TT; (c) azimuthal scans in the -90 +90º angle range for a sample with 1h at 160ºC; open symbols – before TT, solid symbols – after TT. The fit is made with the sample before TT.

Figure 9 Simplified scheme of the stress-induced changes in isotropic PA12 films with flexible amorphous phase. The shaded rectangles represent the crystalline domains of the lamellae. 1 – Random distribution of lamellae in the starting films resulting in spherical SAXS patterns; 2 – Oriented lamellar stacks before TT resulting in two-point scattering patterns; 3 – Tilting of the lamellar stacks after TT producing four-point patterns.

Figure 10 Simplified scheme of the stress-induced changes in PA12 OCs. The shaded rectangles represent the crystalline domains of the lamellae. 4 –Oriented lamellar stacks formed at lower DR resulting in two-point scattering patterns; 5 – Co-existence of two- and four-point patterns at medium DR arranging the scattering elements in macrolattice; 6 - loss of lateral correlation and formation of fibrils with very large L_B.

Table Headers and Footers

Table 1

(Header) Tensile properties of isotropic and oriented PA12 samples after various annealing (OC = oriented cable).

(Footer): [a] Oriented cables displayed two yield points; w.a. = without annealing.

Table 2

(Header) Solid state ^{13}C NMR analysis of PA12 isotropic and oriented samples annealed for 1 h at 160ºC before and after tensile test (aliphatic C region).

(Footers)

[a] The resonances of the corresponding nucleus of α and γ form cannot be separated.

[b] Fitting does not suggest a resonance peak in this region in oriented samples.

(Chemical structure; to be inserted possibly between the header and Table 2)

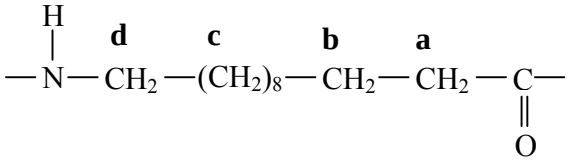

Table 3

(Header): Temperature dependence of the crystallinity indices CI_{total} or ECI, α-CI, γ-CI, and the α/γ polymorph ratio before and after tensile test resulting in sample failure (w.a. = without annealing).

(Footer): [a] No data available.

Table 4

(Header): Unit Cell Vectors and the Corresponding d-Spacings Obtained from the 1D and 2D WAXS Patterns of Isotropic and Oriented PA12 Samples as a Function of Their Initial Annealing Before and After the Tensile Test that Resulted in Sample Failure.

(Footer): [a] The **b** vector of the γ form for some samples was obtained from the meridional (020) reflection of the respective 2D WAXS patterns.

Table 5

(Header): Long Spacing Estimates for Differently Annealed Isotropic and Oriented PA12 Samples Before and After the Tensile Stress Test

(Footers):

[a] The L_B values are determined from the raw SAXS profiles obtained after radial integration of the respective 2D images;

[b] No coherent SAXS scattering.

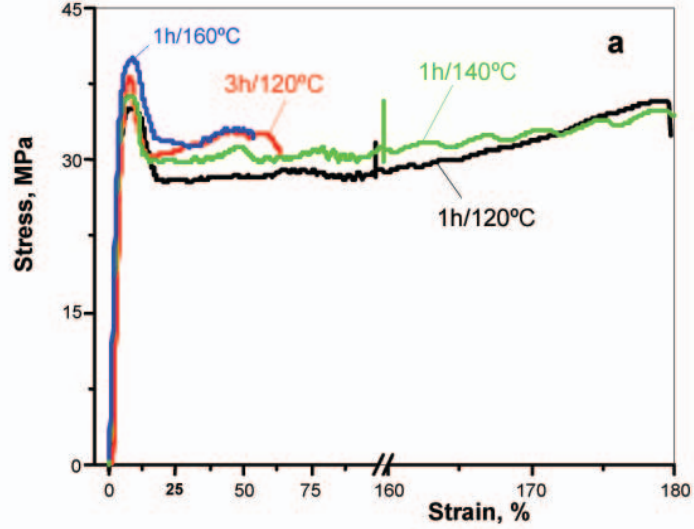
a
1h/160ºC
3h/120ºC
1h/140ºC
1h/120ºC
Stress, MPa
Strain, %
45
30
15
0
0
25
50
75
160
170
180

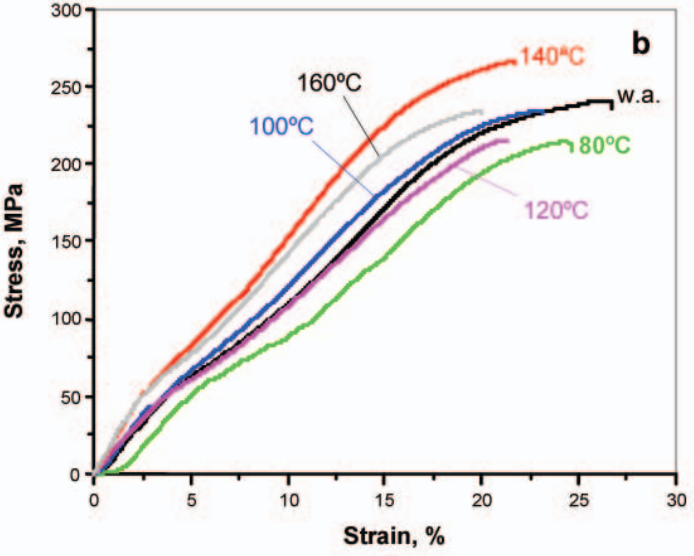
b
140ºC
160ºC
w.a.
100ºC
80ºC
120ºC
Stress, MPa
Strain, %
300
250
200
150
100
50
0
0
5
10
15
20
25
30

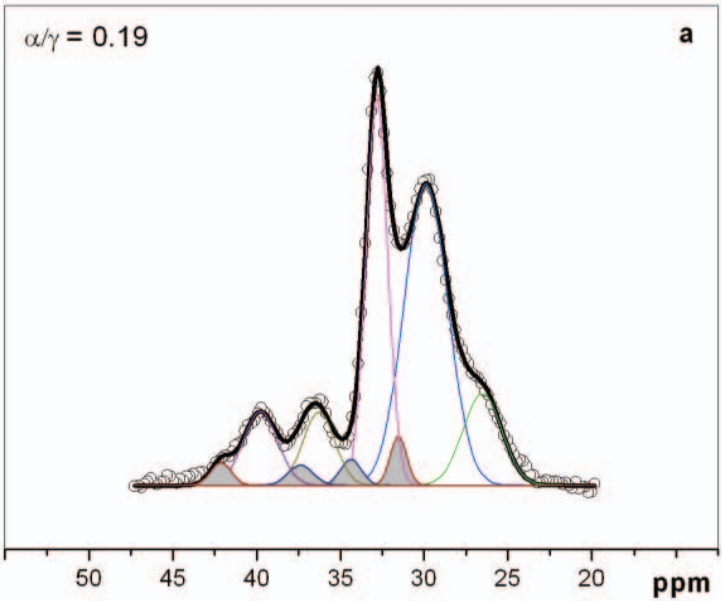
α/γ = 0.19
a
50
45
40
35
30
25
20
ppm

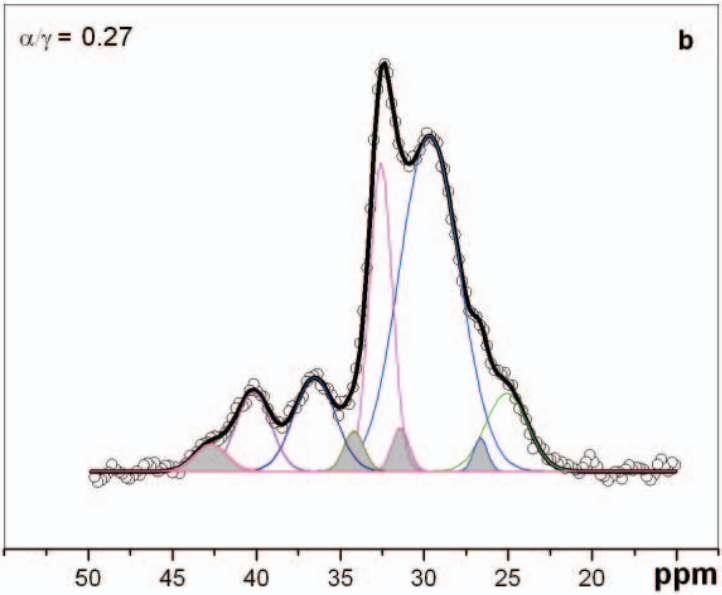
α/γ = 0.27
b
50
45
40
35
30
25
20
ppm

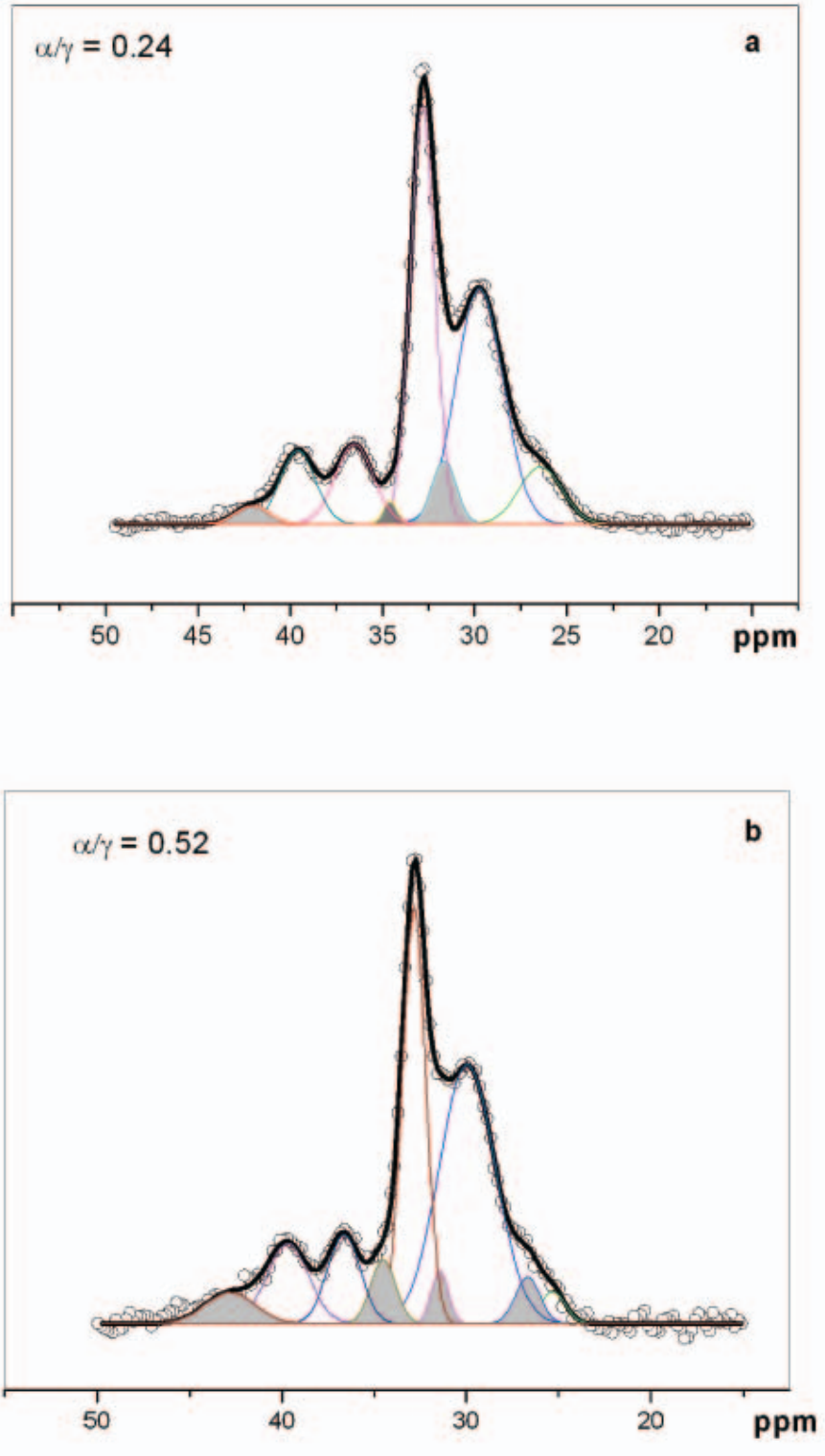
α/γ = 0.24
a
50
45
40
35
30
25
20
ppm
α/γ = 0.52
b
50
40
30
20
ppm

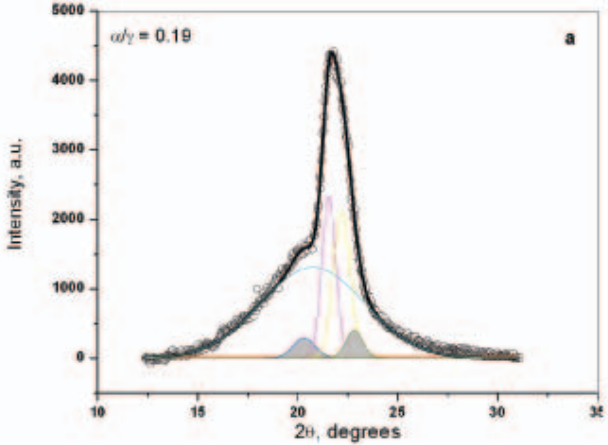
α/γ = 0.19
a
Intensity, a.u.
2θ, degrees

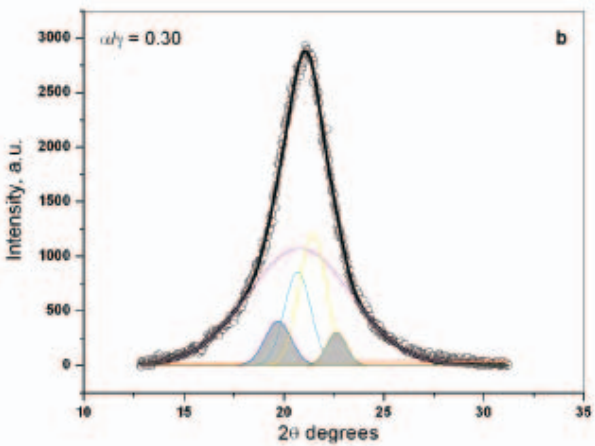
α/γ = 0.30
b
Intensity, a.u.
2θ degrees

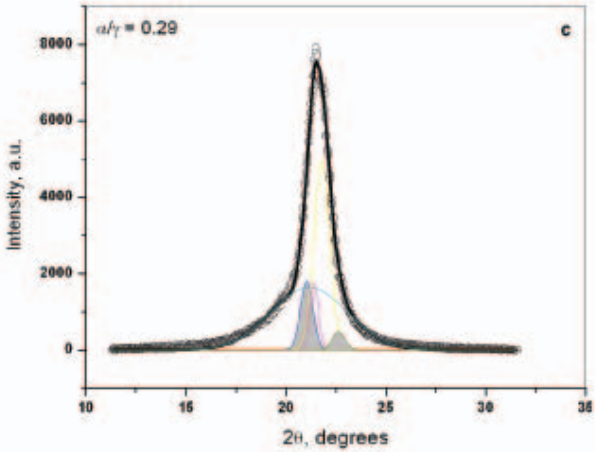
α/γ = 0.29
c
Intensity, a.u.
2θ, degrees

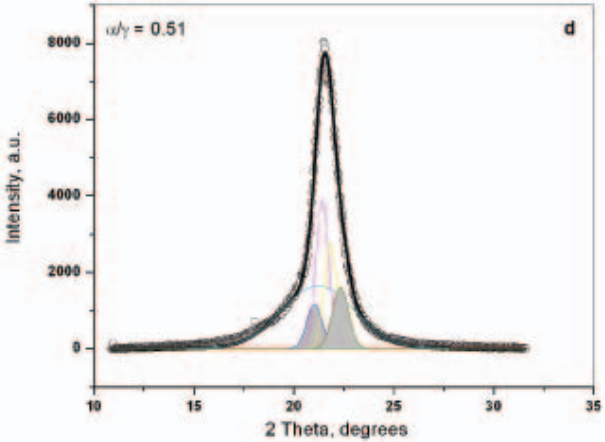
α/γ = 0.51
d
Intensity, a.u.
2 Theta, degrees

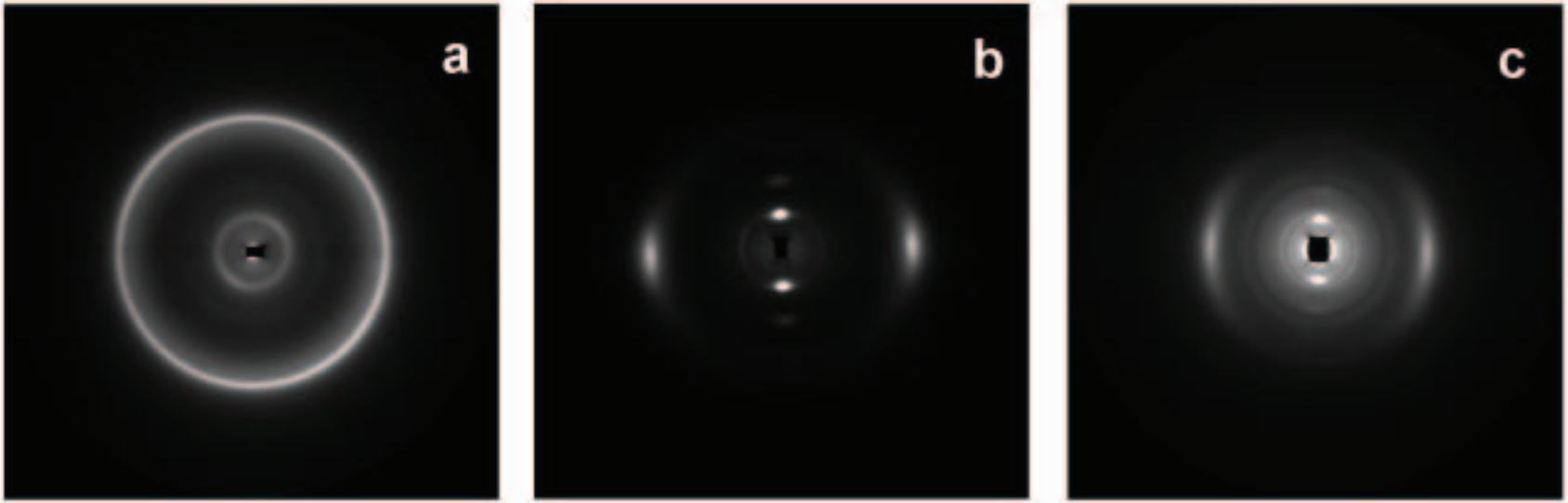
a
b
c

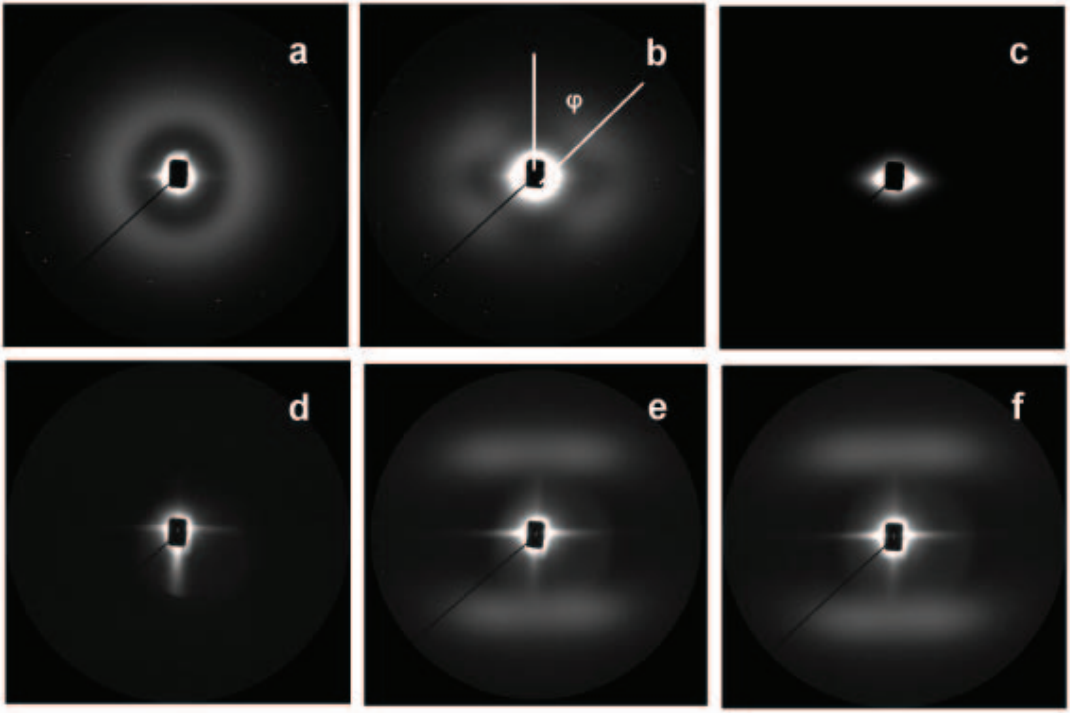
a
b
φ
c
d
e
f

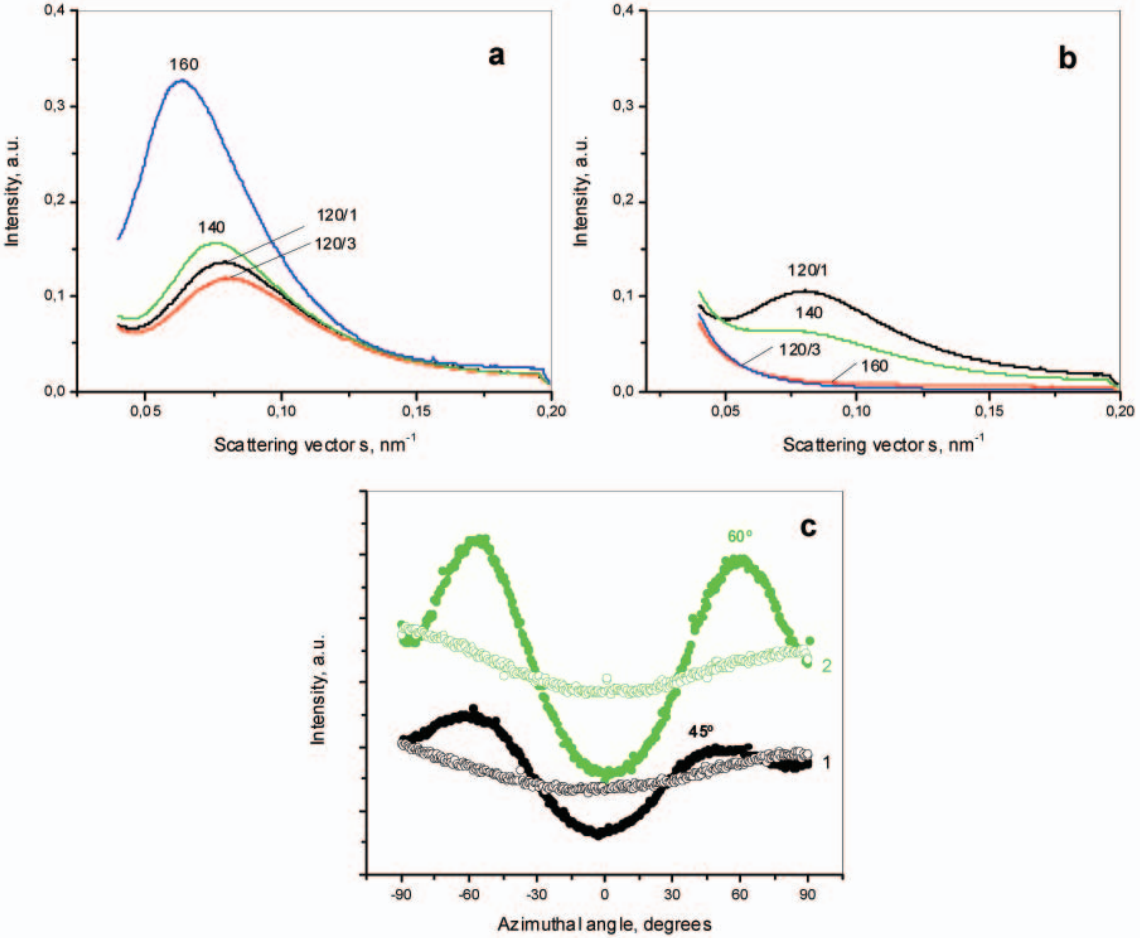
a
160
140
120/1
120/3
Intensity, a.u.
Scattering vector s, nm^{-1}
0,0
0,1
0,2
0,3
0,4
0,05
0,10
0,15
0,20
b
120/1
140
120/3
160
Intensity, a.u.
Scattering vector s, nm^{-1}
c
60°
2
45°
1
Intensity, a.u.
Azimuthal angle, degrees
-90
-60
-30
0
30
60
90

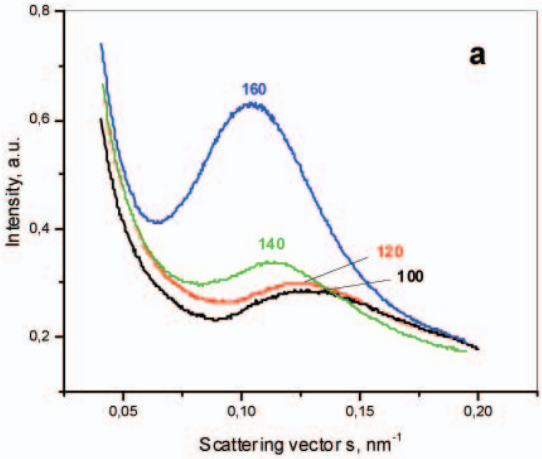
a
160
140
120
100
Intensity, a.u.
0,8
0,6
0,4
0,2
0,05
0,10
0,15
0,20
Scattering vector s, nm-1

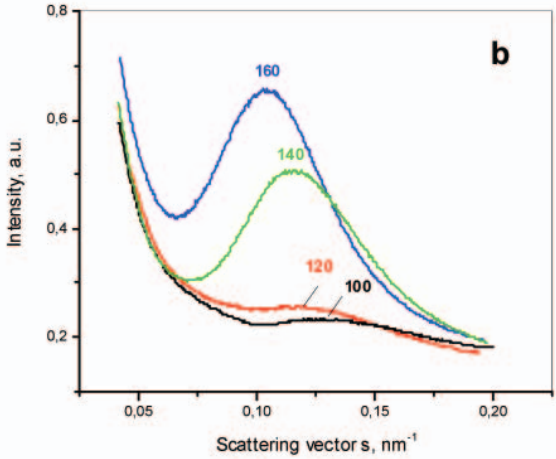
b
160
140
120
100
Intensity, a.u.
0,8
0,6
0,4
0,2
0,05
0,10
0,15
0,20
Scattering vector s, nm-1

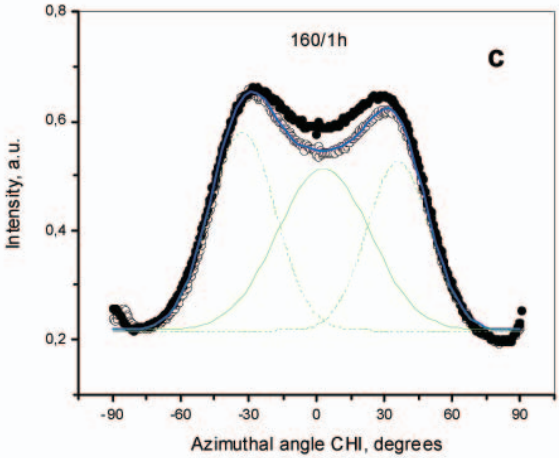
160/1h
c
Intensity, a.u.
0,8
0,6
0,4
0,2
-90
-60
-30
0
30
60
90
Azimuthal angle CHI, degrees

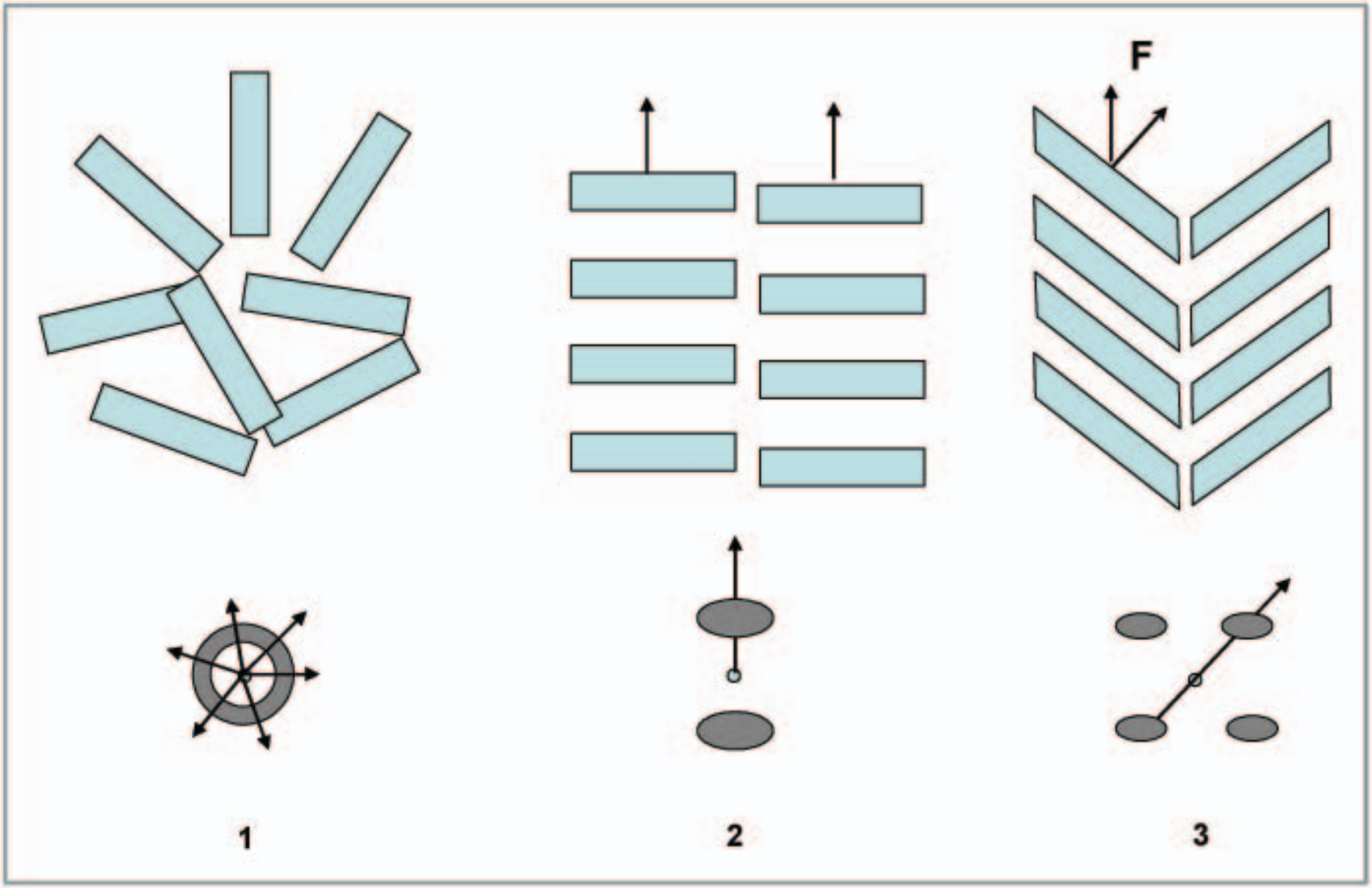
F
1
2
3

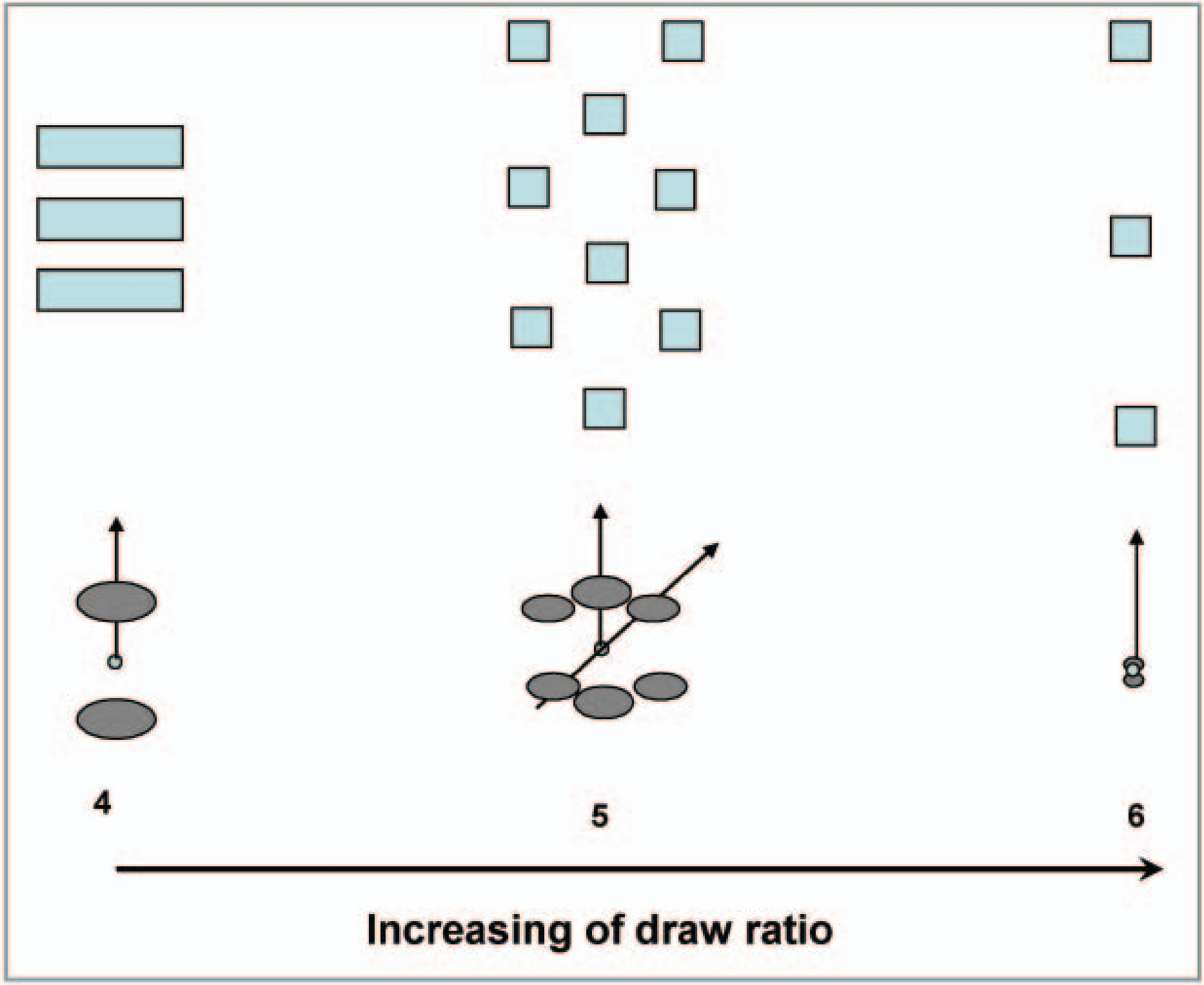
4
5
6
Increasing of draw ratio

Table 1

Sample/ Annealing	*E*, (GPa)	σ_y, MPa[a]	Yield Strain, %	Max. Stress, MPa	Strain at Max. Stress, %	σ_{br}, MPa	ε_{br}, %
PA12 film 120ºC/1h	0.83 ± 0.07	32 ± 3	8.1 ± 0.5	33 ± 10	188 ± 16	33 ± 8	189 ±20
PA12 film 120ºC/3h	1.01 ± 0.10	34 ± 5	6.9 ± 0.1	35 ± 6	7 ± 2	27 ± 6	63 ± 5
PA12 film 140ºC/1h	0.89 ± 0.07	32 ± 1	8.3 ± 0.6	34 ± 6	200 ± 11	35 ± 9	203± 13
PA12 film 160ºC/1h	1.03 ± 0.06	36 ± 1	8.7 ± 0.5	36 ± 3	9 ± 1	28 ± 7	54 ± 6
PA12 OC, w.a.	1.63 ± 0.08	56 ± 1 220 ±2.0	4.2 ± 0.4 18.7 ± 1.0	241± 10	26 ± 3	235 ± 7	27 ± 3
PA12 OC 80ºC/1h	1.23 ± 0.16	53 ± 1 207 ± 2	4.9 ± 0.3 21.3 ± 1.4	215± 6	24 ± 2	209 ± 7	25 ± 2
PA12 OC 100ºC/1h	1.67 ± 0.07	45 ± 1 227 ± 2	2.9 ± 0.2 18.5 ± 1.1	234 ± 3	23 ± 2	233 ± 10	23 ± 3
PA12 OC 120ºC/1h	1.46 ± 0.10	50 ± 2 213 ± 2	3.6 ± 0.2 19.6 ± 1.5	216 ± 8	21 ± 2	214 ± 9	21 ± 2
PA12 OC 140ºC/1h	2.19 ± 0.12	59 ± 2 254 ± 3	2.9 ± 0.1 16.5 ± 0.9	266 ±10	21 ± 3	265 ± 10	22 ± 2
PA12 OC 160ºC/1h	2.24 ± 0.15	58 ± 1 230 ± 3	2.8 ± 0.2 16.5 ± 0.8	234 ± 8	20 ± 1	233 ± 11	20 ± 1

Table 2

NMR resonances	Samples				
	PA12 from [19]	PA12 film	PA12 film, after TT	PA12 OC	PA12 OC, after TT
	Chemical shifts, ppm				
b γ form (γ' form)	~28 (~27)	26.5[a]	25.1	26.4[a]	25.3
b (α form)	27.3		26.7		26.7
c gauche γ form **c** gauche γ'-form)	30.3 30.8	29.9	29.7	29.7	30.0
c gauche (α form)	30.9	31.6	31.4	31.6	31.4
c trans (γ form) **c** trans (γ' form)	33.6 33.1	32.8	32.5	32.8	32.8
c trans (α form)	34.2	34.4	34.2	34.6	34.5
a (γ form) **a** (γ' form)	37.3 37.0	36.3	36.5	36.5	36.6
a (α form)	38.9	37.4	-[b]	-[b]	-[b]
d (γ form) **d** (γ' form)	39.8 40.3	39.8	40.2	39.5	39.9
d (α form)	43.0	42.2	42.7	42.1	42.8
α / γ content	**-**	**0.19**	**0.27**	**0.24**	**0.52**

Table 3

Sample/ Annealing temperature, ºC	Before tensile test				After tensile test			
	CI_{α} %	CI_{γ} %	CI_{Total} or ECI	α/γ content	CI_{α} %	CI_{γ} %	CI_{Total} or ECI	α/γ content
PA12 Isotropic Films								
120/1h	4.1	26.9	31.0	0.18	12.3	26.1	38.4	0.47
120/3h	6.6	27.0	33.6	0.24	9.2	27.5	36.7	0.33
140/1h	7.5	26.0	33.5	0.29	10.1	28.3	38.4	0.36
160/1h	6.0	31.3	37.3	0.19	9.1	30.2	39.3	0.30
PA12 Oriented Cables								
w.a.	8.4	33.4	41.8	0.25	-	-	-	- [a]
80/1h	9.4	31.9	41.3	0.29	14.9	28.3	43.1	0.53
100/1h	12.8	38.0	50.8	0.34	19.4	32.9	52.3	0.59
120/1h	14.5	36.6	51.1	0.39	20.9	32.4	53.3	0.65
140/1h	13.3	39.3	52.6	0.34	18.2	32.9	51.1	0.55
160/1h	11.5	37.8	49.3	0.30	17.6	33.9	51.6	0.52

Table 4

Annealing, ºC	$d_{\alpha 200}$		$d_{\alpha 002}$		$d_{\gamma 200}$		$d_{\gamma 001}$		$d_{\gamma 020}$	
	Before	**After**	**Before**	**After**	**Before**	**After**	**Before**	**After**	**Before**	**After**
PA12 isotropic film										
At 120/1h	4.28	4.36	3.82	3.90	4.02	4.14	3.96	4.02	14.00[a]	13.68
At 120/3h	4.25	4.36	3.82	3.86	4.02	4.12	3.92	4.02	-	-
At 140/1h	4.22	4.32	3.83	3.86	4.04	4.14	3.91	4.00	-	-
At 160/1h	4.21	4.38	3.79	3.82	4.01	4.18	3.90	4.03	13.34	12.99
PA12 orient. cables										
Without annealing	4.26	-	3.83	-	4.09	-	3.98	-	13.98	13.02
At 80/1h	4.22	4.20	3.84	3.88	4.07	4.07	3.96	3.99	-	-
At 100/1h	4.28	4.26	3.89	3.91	4.09	4.08	4.00	3.99	-	-
At 120/1h	4.15	4.13	3.89	3.90	4.04	4.04	3.98	3.96	-	-
At 140/1h	4.14	4.13	3.89	3.92	4.09	4.09	3.97	4.01	-	-
At 160/1h	4.11	4.11	3.82	3.87	4.03	4.03	3.96	3.96	13.50	13.12

Table 5

	Annealing at, ºC	L_B estimates[a], Å	
		Before	**After**
Isotropic PA12 films	120/1h	126	122
	120/3h	128	-[b]
	140/1h	130	124
	160/1h	160	-
Oriented PA12 cables	w.a.	-[b]	-[b]
	80/1h	-[b]	--[b]
	100/1h	77	78
	120/1h	78	78
	140/1h	84	85
	160/1h	96	96